

Jan Liu*, Mathias Reisbeck, Oliver Hayden

Investigation of mechanical and magnetophoretic focusing for magnetic flow cytometry

Abstract: As an alternative to optical flow cytometry, magnetic flow cytometry has emerged in recent years for single cell analysis with sheath-less flow conditions. Instead of measuring scattered light, magnetic fields of magnetically-labeled cells are recorded and analyzed. To determine microfluidic opportunities to manipulate cell trajectories for in-situ cell focusing we use mechanical guiding structures and magnetophoretic forces. A 3D-microfluidic particle simulation has been implemented that revealed parameters ensuring the crucial balance between hydrodynamic drag and magnetophoretic forces. Experimental measurements verified the 3D particle tracking simulation.

Keywords: Magnetic flow cytometry, cell focusing, particle focusing, magnetophoresis, microfluidics

<https://doi.org/10.1515/cdbme-2019-0089>

1 Introduction

Despite the broad applicability of flow cytometry for single cell analysis, clinical instruments are still limited to specialized laboratories due to workflow complexity, laborious sample preparation, and high capital invest [1, 2]. Magnetic flow cytometry has emerged as an economically viable solution for non-optical detection of cells in opaque blood. Time-of-flight (TOF) magnetic sensing of immunomagnetically-labeled cells rolling inside a microfluidic system offers great potential for single cell analysis in point-of-care (POC) settings [3, 4]. The cells are pulled to the substrate of a microfluidic channel by a permanent magnet positioned under the channel and are dragged through the channel by hydrodynamic drag forces exerted by the moving fluid.

*Corresponding author: **Jan Liu:** Heinz-Nixdorf-Chair of Biomedical Electronics, Technical University of Munich, Einsteinstr. 25, Munich, Germany, e-mail: jan.liu@tum.de
Mathias Reisbeck, Oliver Hayden: Heinz-Nixdorf-Chair of Biomedical Electronics, Munich, Germany

A giant magneto-resistance (GMR) sensor measures the weak magnetic fields generated by the immunomagnetically-labeled cells by a change in electrical resistance. A controlled movement of the cells over the sensor ensuring proper spatial distances to each other is essential in order to record signal patterns for multiparametric sensing and to avoid coincidence signals [2, 4, 5].

This can be achieved by implementing 3D chevron-shaped structures into the microchannel covering a certain ratio of the channel width (coverage ratio). As a first step, the channel is filled with the cell suspension at a high flow rate. Second, the flow is stopped and the magnet pulls the cells onto substrate surface. Third, the flow rate is set to a specific value where magnetic and hydrodynamic forces are in balance. An illustration of this method is given in Figure 1. The partitioning into different enrichment stages ensures the ability to adapt to different cell concentrations. For high concentrations, the stages with small coverage ratios are considered as they only focus small ratios of cells and vice versa. As the guiding structures are lower than the channel height, all non-magnetic (non-labeled) cells pass the structures with unaffected trajectories dragged by the laminar flow [6].

This work aims for implementation of numerical simulations and tracking algorithms to optimize and characterize design patterns for guiding of immunomagnetically-labeled cells based on the balancing of hydrodynamic and magnetic forces.

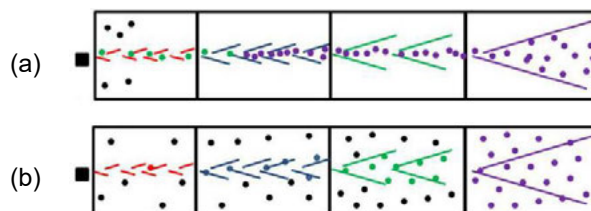


Figure 1 Stochastically distributed cells after step one and two (a), continuous stream of aligned particles focused to the channel center (b) [6].

2 Materials and methods

2.1 Prototyping of microfluidic channels

3-inch silicon wafers (Silicon Materials e.K.) were coated with a layer of SU-8 3050 (MicroChem Corp.) at a spin speed of 800 rpm. After a soft-baking step, the photoresist was exposed to a 365 nm UV light source for 120 s through a patterned photomask (KOENEN GmbH). A post-exposure baking step followed, before the wafers were developed for 20 min [7–9]. To obtain an elastomeric replica of the mold as depicted in Figure 2, the pre-polymer polydimethylsiloxane (PDMS) base was mixed with a cross-linking agent in a 10:1 ratio before it was poured onto the SU-8 master molds positioned in petri dishes. After curing, the pieces of PDMS containing the channels were removed from the petri dishes. Single microfluidic channels were cut and holes were punched with sharpened cannulas (Nordson EFD) [10].

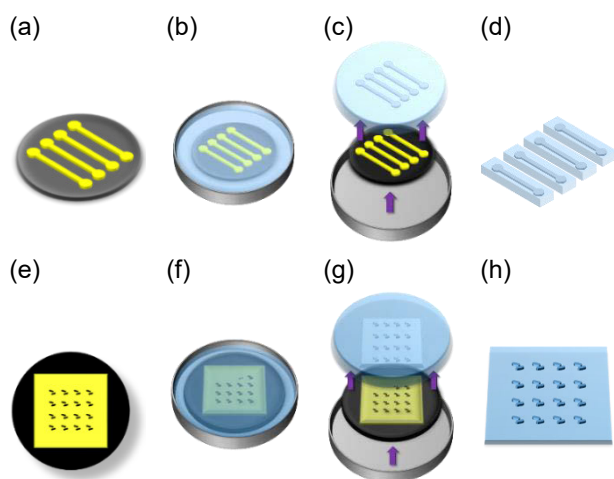


Figure 2 SU-8 structured wafer (a, e), PDMS covering the master mold for microchannels (b), removing cured piece of PDMS (c, g), single microfluidic channels (d), PDMS covering the master mold for guiding structures (f), piece of PDMS with 3D guiding structures (h).

The guiding structures were fabricated from PDMS with an inverted molding process. After the lithographic process (spin speed 3000 rpm, UV light exposure time 70 s), the wafers were covered with SU-8 leaving cavities for PDMS casting in a petri dish. In this way, 3D guiding structures with variable aspect ratios were fabricated as can be seen in Figure 2.

Bonding of the channels to the structured PDMS piece was performed using a stamp-and-stick (SAS) transfer bonding technique [11]. Freshly mixed PDMS in a 10:1 ratio of base and curing agent was poured on a 3-inch silicon wafer and spun at 10 000 rpm for 1–2 min which resulted in a thin

layer of uncured PDMS with a thickness of a few micrometers. The PDMS microchannels were placed on the coated wafer and inked with uncured PDMS. With the help of a stereomicroscope, the channels were positioned over the structures and cured at 60 °C for 60 min to obtain the assembled device as can be seen in Figure 3.

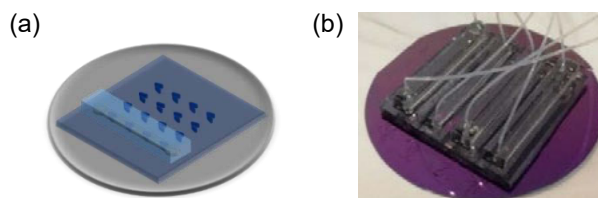


Figure 3 Scheme (a) and image (b) of assembled microchannel on a wafer.

2.2 Experimental setup

A syringe pump (Fusion 4000, Chemyx Inc.) injected the analyte suspension into the microfluidic *via* PTFE tubings (inner diameter 0.3 mm, outer diameter 0.8 mm, Reichelt Chemietechnik GmbH) which were connected to the inlet and outlet holes of the structured PDMS channels. A Neodymium-iron-boron permanent magnet with a size of 75 × 50 × 10 mm (ChenYang Technologies GmbH) was centered underneath, with a distance of 5 mm resulting in a magnetic field density of 140 mT, determined by a Gaussmeter (CYHT201, ChenYang Technologies GmbH), and a calculated magnetic field gradient of 4 T/m. It is assumed that only field components in z-direction are effective, resulting in a unidirectional alignment of magnetic analytes. A microscope (DM6 M, Leica Microsystems GmbH) together with a CMOS camera (DFC9000 GT, Leica Microsystems GmbH) was used to record the analyte movement with a rate of 38.5 fps. Magnetic particles (micromer-M, micromod GmbH) with a diameter of 6 μm were used as analytes. The magnetic moment per particle is given on the datasheet as 6×10^{-13} Am², which is in the same order of labeled cells.

Red blood cells (RBCs) were sphered and fixated using a modified PBS solution containing SDS and glutaraldehyde (Sigma-Aldrich). The immunomagnetic labeling of RBCs was done in two steps via Glycophorin A (CD235a). First, FITC-conjugated CD235a-antibodies (Miltenyi Biotec GmbH) were attached to the RBCs, second, magnetic nanoparticles (Anti-FITC Micro Beads, Miltenyi Biotec GmbH) were attached to the FITC molecules. GDPTlab 1.0, a particle tracking software, implemented in MATLAB, was used that is able to track 3D positions of cells based on microscopic images [12].

2.3 Microfluidic particle simulation

To model the interaction between particle and guiding structures, a 3D-microfluidic particle simulation algorithm was implemented in MATLAB. First, COMSOL’s Computational Fluid Dynamics (CFD) module is used to calculate the velocity profile around the chevron barriers. Second, the results are imported into the particle simulation algorithm. In each simulation step, the velocity of a particle v_p is calculated by evaluating magnetic forces F_m exerted by a magnetic field in z-direction, hydrodynamic drag forces F_d and gravitational forces F_g acting on the particles:

$$m \frac{dv_p}{dt} = F_m + F_d + F_g.$$

As all forces involved are in the same order of magnitude, they all need to be accounted for. The resulting velocity is used to determine the particle position in the next simulation step. The surface of a particle is represented by a number of discrete points [13]. Whenever a collision is detected, i.e. at least one of the discrete points is located inside a wall structure, the particle’s position is shifted by a specific shifting vector. That vector is directed from the centroid of all points inside the wall to the particle’s centroid and has a magnitude that is just enough to shift the particle outside the wall again.

3 Results

3.1 Simulation results

Different flow rates, structure heights, and guiding angles, i.e. the angle of the guiding structures with respect to the flow direction, were investigated. 6 μm sized magnetic and non-magnetic particles in 1500 μm and 1000 μm wide channels were tested. For all simulations, the particles were exposed to a magnetic field gradient of 4 T/m. In Figure 4 a snapshot of the trajectory simulation with MATLAB is shown. The flow rates that allow guiding of magnetic particles and leave the non-magnetic particles unaffected are chosen between 1.5 to 3.0 $\mu\text{l/s}$ for 1500 μm wide channels and between 1.0 to 2.0 $\mu\text{l/s}$ for 1000 μm wide channels. Guiding structure heights of 10, 25, and 50 μm were tested in a 1500 μm wide channel and a constant flow rate of 3.0 $\mu\text{l/s}$ matching magnetic flow cytometry conditions with blood cell biomarkers.

We observe that focusing works well for 50 μm high structures whereas for 10 μm and 25 μm particles pass the structures without being affected. This is due to the flow velocity profile that exerts drag forces dominating the

magnetic forces. However, for the given simulation conditions of 3.0 $\mu\text{l/s}$ and a field gradient of 4 T/m, guiding is still possible with a structure height to particle diameter ratio <4 when using multiple pairs of structures. The influence of the guiding structure angles was tested for a channel width of 1000 μm and 50 μm line heights. Guiding is achieved with lines fabricated at an angle of 7.5° to the flow direction and flow rates from 0.7 to 1.0 $\mu\text{l/s}$. With angles of 15° and 30° the flow regime for guiding increases from 1.0 and 2.0 $\mu\text{l/s}$ to 1.0 and 3.0 $\mu\text{l/s}$, respectively. Further increase of the angle does not change the guiding efficiency significantly.

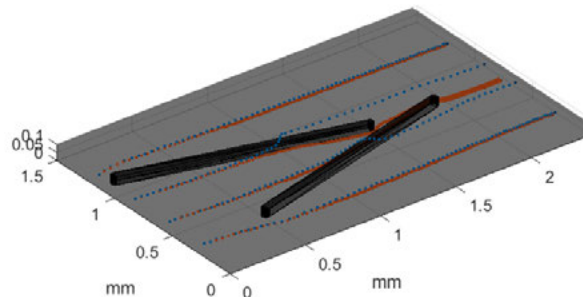


Figure 4 Simulated particle trajectories of 6 μm magnetic particles (orange) and nonmagnetic particles (blue) in a 1500 μm wide channel with 50 μm high guiding structures, starting in 250 μm height, at a flow rate of 0.5 $\mu\text{l/s}$.

3.2 Experimental results

For both channel widths of 1500 μm and 1000 μm , the best focusing behavior was obtained using a flow rate ≤ 1.0 $\mu\text{l/s}$. In Figure 5 (a), statistics on the particle exit with respect to the channel width of 1500 μm are shown.

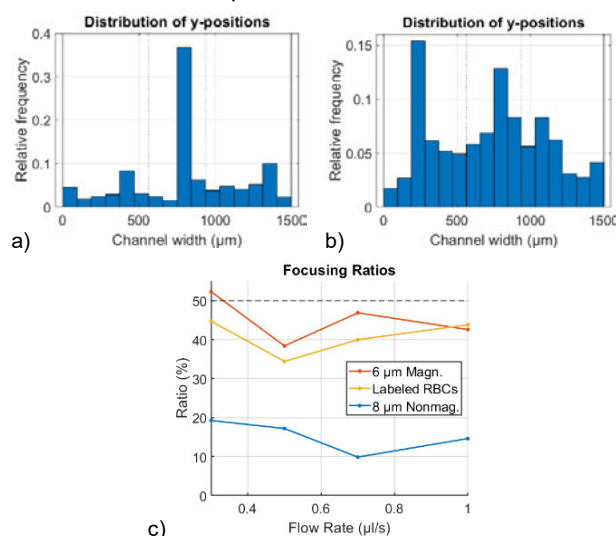


Figure 5 Exit coordinates for 6 μm magnetic particles (a) and 8 μm non-magnetic particles (b), guiding efficiency for different analytes (c).

About 43 % percent of the particles are focused which indicates a quite good focusing behavior (coverage ratio 50%). Similar results were found with immunomagnetically-labeled RBCs in the 1500 μm wide channel. However, the guiding efficiency was reduced which could be related to lower magnetic moments compared to polymeric magnetic beads.

4 Discussion

The simulated particle trajectories follow the experimentally-obtained particle trajectories very well as shown in Figure 6.

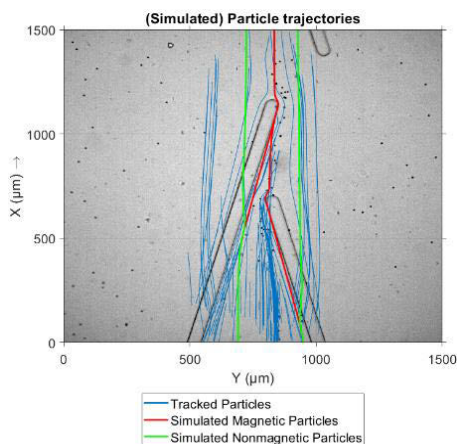


Figure 6 Simulated and experimentally-tracked particle trajectories.

However, in the microfluidic experiments, we observe that fractions of the magnetic particles are not guided well. This result might be related to a distribution of magnetic moments of beads and effects over a row of guiding structures a stepwise increase of the z-position. Thus, lift from the substrate due to hydrodynamic drag forces occurs that leads to loss of guiding. The simulation has revealed that flow rates $\leq 2.0 \mu\text{l/s}$ and $\leq 3.0 \mu\text{l/s}$ work well for 6 μm magnetic particles in 1500 μm and 1000 μm wide channels, respectively, and a constant 100 μm channel height with guiding lines at 15° . Simulated and experimental results matched well for the guiding efficiency with respect to the line heights.

5 Conclusion and future work

Here, a model based on numerical simulation and particle trajectory analysis has been developed for mechanical and magnetophoretic cell focusing. The developed algorithms can thus be used to optimize and fine-tune aspect ratio and design of chevron structures with respect to experimental parameters such as flow rates and magnetization of analytes.

Geometrical and flow requirements were simulated and experimentally verified to guide magnetized particles and cells in laminar flow conditions with aspect ratios between guiding structures and channel dimensions close to real-world, which supports the optimization of pre-analytical steps for magnetic flow cytometry.

Author Statement

Research funding: The author state no funding involved.
Conflict of interest: Authors state no conflict of interest.

References

- [1] J. P. Robinson and M. Roederer, "HISTORY OF SCIENCE. Flow cytometry strikes gold," *Science (New York, N.Y.)*, vol. 350, no. 6262, pp. 739–740, 2015.
- [2] M. Reisbeck et al., "Magnetic fingerprints of rolling cells for quantitative flow cytometry in whole blood," *Scientific reports*, vol. 6, p. 32838, 2016.
- [3] M. Helou et al., "Time-of-flight magnetic flow cytometry in whole blood with integrated sample preparation," *Lab on a chip*, vol. 13, no. 6, pp. 1035–1038, 2013.
- [4] D. Issadore and R. M. Westervelt, *Point-of-Care Diagnostics on a Chip*. Berlin, Heidelberg: Springer Berlin Heidelberg, 2013.
- [5] H. Lee, T.-H. Shin, J. Cheon, and R. Weissleder, "Recent Developments in Magnetic Diagnostic Systems," *Chemical reviews*, vol. 115, no. 19, pp. 10690–10724, 2015.
- [6] M. Reisbeck et al., "Hybrid integration of scalable mechanical and magnetophoretic focusing for magnetic flow cytometry," *Biosensors & bioelectronics*, vol. 109, pp. 98–108, 2018.
- [7] J. R. Anderson et al., "Fabrication of Topologically Complex Three-Dimensional Microfluidic Systems in PDMS by Rapid Prototyping," *Analytical chemistry*, vol. 72, no. 14, pp. 3158–3164, 2000.
- [8] SU-8 mold lithography - Elveflow. [Online] Available: <https://www.elveflow.com/microfluidic-tutorials/soft-lithography-reviews-and-tutorials/introduction-in-soft-lithography/su-8-mold-lithography/>. Accessed on: Jul. 05 2018.
- [9] R. Martinez-Duarte and M. Madou, "SU-8 Photolithography and Its Impact on Microfluidics," in *Microfluidics and nanofluidics handbook: Fabrication, implementation, and applications*, S. Chakraborty and S. K. Mitra, Eds., Boca Raton, FL: CRC Press, 2012, pp. 231–268.
- [10] J. C. McDonald et al., "Fabrication of microfluidic systems in poly(dimethylsiloxane)," *Electrophoresis*, vol. 21, no. 1, pp. 27–40, 2000.
- [11] S. Satyanarayana, R. N. Karnik, and A. Majumdar, "Stamp-and-stick room-temperature bonding technique for microdevices," *J. Microelectromech. Syst.*, vol. 14, no. 2, pp. 392–399, 2005.
- [12] R. Barnkob, C. J. Kähler, and M. Rossi, "General defocusing particle tracking," *Lab on a chip*, vol. 15, no. 17, pp. 3556–3560, 2015.
- [13] J. Wang, V. G. J. Rodgers, P. Brisk, and W. H. Grover, "MOPSA: A microfluidics-optimized particle simulation algorithm," *Biomechanics*, vol. 11, no. 3, p. 34121, 2